

## Fragment-Based Discovery of BACE1 Inhibitors Using Functional Assays<sup>‡</sup>

Robert Godemann,<sup>\*,§</sup> James Madden,<sup>||</sup> Joachim Krämer,<sup>§</sup> Myron Smith,<sup>||</sup> Ulrike Fritz,<sup>§</sup> Thomas Hesterkamp,<sup>§</sup> John Barker,<sup>||</sup> Sabine Höppner,<sup>⊥</sup> David Hallett,<sup>||</sup> Andrea Cesura,<sup>§</sup> Andreas Ebnet,<sup>§</sup> and John Kemp<sup>§</sup>

<sup>§</sup>Evotec AG, Schnackenburgallee 114, 22525 Hamburg, Germany, <sup>||</sup>Evotec Ltd., 114 Milton Park, Abingdon, Oxfordshire OX14 4SA, U.K., and <sup>⊥</sup>Proteros biostructures GmbH, Am Klopferspitz 19, D-82152 Planegg-Martinsried, Germany

Received June 23, 2009; Revised Manuscript Received September 7, 2009

**ABSTRACT:** Novel nonpeptidic inhibitors of  $\beta$ -secretase (BACE1) have been discovered by employing a fragment-based biochemical screening approach. A diverse library of 20000 low-molecular weight compounds were screened and yielded 26 novel hits that were confirmed by biochemical and surface plasmon resonance secondary assays. We describe here fragment inhibitors cocrystallized with BACE1 in a flap open and flap closed conformation as determined by X-ray crystallography.

Beta secretase (BACE1)<sup>1</sup> catalyzes the rate-limiting step in the production of the  $\beta$ -amyloid peptide (A $\beta$ ) and amyloid plaque formation in Alzheimer's disease (AD). For this reason, many biopharmaceutical companies have been pursuing the discovery of BACE1 inhibitors for the treatment of AD. However, it soon became apparent that BACE1 poses great challenges in delivering potent, small-molecule inhibitors that are both orally bioavailable and able to cross the blood–brain barrier. This has had an impact on the progression of small-molecule inhibitors into the clinic.

Fragment-based drug discovery (FBDD) is a new approach to identifying such small-molecule inhibitors (1, 2) and, furthermore, has proven to be particularly well suited for technically challenging targets such as BACE1. Previous work has shown that low-molecular weight hits with millimolar affinities could be identified (3–5) and efficiently developed into potent leads with nanomolar affinity and druglike properties (6, 7). In the majority of the published FBDD campaigns against BACE1, biophysical screening techniques, including NMR, high-throughput crystallography, surface plasmon resonance (SPR), and tethering (8), have been applied for primary fragment screening. Typically therein, focused fragment libraries have been used, containing only a limited number of fragments and, hence, restricted chemical diversity.

Functional assays allow the screening of a larger chemical diversity space. Homogeneous, miniaturized fluorescence polarization assays have proven to be robust and cost-effective solutions for drug discovery. However, such assay results must be thoroughly scrutinized if applied to the screening of compounds at high concentrations, which is a prerequisite for FBDD campaigns. The confirmed fragment hits can subsequently be developed into more potent and druglike molecules using detailed

structural information about the protein–fragment complexes generated by, for example, X-ray crystallography.

The three-dimensional (3D) structure determination of the BACE1 ectodomain revealed a bilobal structure typical for eukaryotic aspartic proteases with the catalytic aspartate residues Asp32 and Asp228 located in the substrate binding cleft between the N-terminal and C-terminal lobes (9). The active site is partially covered by a flexible hairpin loop termed the “flap”. In complex with peptidomimetic inhibitors, the flap is approximately 4.5 Å displaced toward the substrate binding cleft compared to the apo structure (10, 11). Fragment inhibitors with millimolar affinity in a complex with BACE1 have been reported to bind in the flap open conformation of the enzyme interacting with the catalytic aspartate residues (4, 5). In contrast, an entirely new mode of binding of a low micromolar BACE1 inhibitor was recently reported without catalytic aspartate engagement (12).

We report here a fragment screening approach that combines a highly diverse fragment library with sensitive biochemical screening methods (13). We show that this system is suitable for identifying low-affinity but efficient small-molecule inhibitors of BACE1. The X-ray structures of the resulting protein–ligand complexes reveal valuable insights into the detailed binding mode of the fragments, providing the basis for a rational structure-guided medicinal chemistry optimization program.

### EXPERIMENTAL PROCEDURES

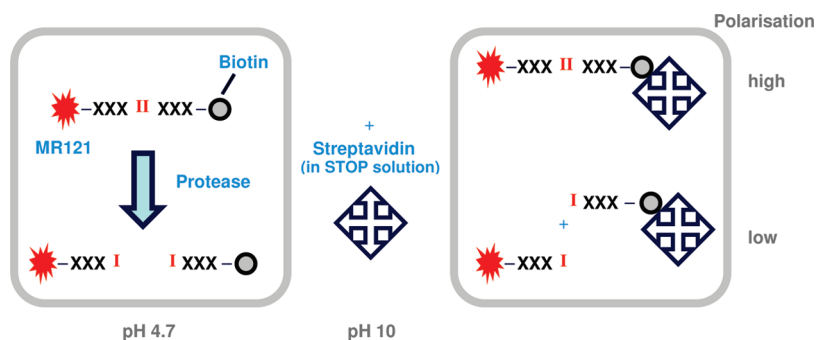
**Primary BACE1 Screening Assay.** For fragment screening, the BACE1 protein was purchased from R&D Systems. Briefly, BACE1 (20 nM) was added to the compounds (1 mM) and equilibrated for 30 min in 50 mM sodium acetate buffer (pH 4.8), 100 mM NaCl, 0.05% BSA, and 0.05% Pluronic F-127. In a subsequent step, the enzymatic reaction was started by addition of 150 nM fluorescently labeled biotinylated substrate peptide. The peptide biotin-SEVNLDAEFR-K(MR121)-RR is derived from the “Swedish mutation” (14) of the amyloid precursor protein and is cleaved by BACE1 between leucine and aspartic acid, as indicated. After incubation for 45 min at 37 °C, the reaction was stopped by addition of 300 nM streptavidin in 500 mM Tris-HCl (pH 10). Following another equilibration step, the assay was measured by help of a confocal fluorescence correlation spectroscopy (FCS) reader.

<sup>‡</sup>X-ray crystal structure coordinates have been deposited in the Protein Data Bank (PDB) as entries 3HW1 for the BACE1–Compound 1 complex and 3HVG for the BACE1–Compound 8 complex.

<sup>\*</sup>To whom correspondence should be addressed. Phone: +49-(0)40-56081299. Fax: +49-(0)40-56081440. E-mail: robert.godemann@evotec.com.

Abbreviations: SPR, surface plasmon resonance; NMR, nuclear magnetic resonance; FP, fluorescence polarization; BACE1,  $\beta$ -site amyloid precursor protein cleaving enzyme, isoform 1; A $\beta$ , amyloid  $\beta$ -peptide; LE, ligand efficiency; BBB, blood–brain barrier; TPSA, topological polar surface area; ADME, absorption, distribution, metabolism, and excretion; rmsd, root-mean-square deviation.

Scheme 1: Fluorescence Polarization BACE1 Assay



**Secondary BACE1 Assay.** The  $\beta$ -galactosidase enzyme complementation assay (15) is commercially available (HitHunter  $\beta$ -secretase assay) from DiscoverX/GE Healthcare. Experiments were performed essentially according to the manufacturer's instruction with slight modifications for high-concentration compound testing. The BACE1 ectodomain (110 nM) was preincubated at room temperature for 30 min with the fragments (0.03–2 mM). The reaction was started via addition of the cyclic substrate (ED) and the mixture incubated in the provided reaction buffer (pH 4.5) for 60 min at 37 °C. The final DMSO concentration was 3.3%. The BACE1 cleavage reaction was stopped by a pH shift, and the  $\beta$ -galactosidase reaction was started via addition of the  $\beta$ -galactosidase solution (EA) consisting of 30 mM Tris-HCl (pH 8) and 6 mM 2-nitrophenol  $\beta$ -D-galactopyranoside (ONPG) in 100 mM Na<sub>3</sub>PO<sub>4</sub> buffer (pH 7.3). Absorbance at 420 nm was recorded for 2–8 h. A possible interference of the compound with the read-out was tested via addition of the compound after the reaction had been stopped by the pH shift. For both assay setups, the concentration response curve was normalized against maximal inhibition of the reaction achieved with the BACE1 inhibitor IV from Calbiochem. Data evaluation was done with Excel Fit (version 4.1, IDBS Limited). IC<sub>50</sub> values were determined by using the following equation:

$y = A + B - A / 1 + \left(\frac{C}{x}\right)^D$  where  $y$  is the assay signal,  $x$  the compound concentration,  $A$  the final minimum  $y$  value,  $B$  the final maximum  $y$  value,  $C$  the IC<sub>50</sub>, and  $D$  the slope of the curve. In case of incomplete inhibition,  $A$  was fixed to zero.

**Surface Plasmon Resonance (SPR) BACE1 Assay.** Interaction analysis was performed as an inhibition in a solution assay (3) on CM5 sensor chips on a Biacore 3000 device (GE Healthcare). The substrate analogue inhibitor (SAI) KTEEI-SEVN-statin-VAEF (Bachem Holding AG, catalog no. H-4848) was dissolved in water and diluted to 0.2 mg/mL in 10 mM sodium acetate (pH 4.0) for immobilization. Contact time for immobilization of SAI was 10 min using 10 mM HEPES, 150 mM NaCl, and 0.005% Tween 20 (pH 7.4) as the running buffer. A scrambled version of SAI, peptide KFES-statin-ETIAEVENV (Peter Henklein, Berlin, Germany), was used in the reference flow cell for online reference subtraction. The SPR signal after immobilization of both peptides was approximately 300 units. The running buffer for all binding and inhibition experiments was composed of 25 mM sodium acetate, 200 mM sodium chloride, 0.005% Tween 20, and 5% DMSO (final pH of 4.5). The recombinant human BACE1 ectodomain was applied at 22 nM and preincubated with the small molecule at different concentrations. The mixture was injected for 7 min over the SAI-modified sensor chip surface with a flow rate of 10  $\mu$ L/min at 25 °C. Regeneration was performed with 5  $\mu$ L of 50 mM Tris-HCl and

0.5% SDS (pH 8.5). Data evaluation was done with GraphPad Prism (version 5.01, GraphPad Software Inc.).

**Protein Expression and Structure Determination.** For SPR, the human BACE1 fragment of residues 14–453 (Swissprot numbering, entry P56817) was utilized. A corresponding gene with optimized codon usage for *Escherichia coli* was synthesized (GENEART AG, Regensburg, Germany) and used for protein expression. Purification was performed as described in ref 16 from inclusion bodies followed by refolding and tag cleavage. Crystal structures of Compounds 1 and 8 were obtained by utilizing refolded BACE1 protein and crystallization conditions as described previously (17). Crystals were obtained by vapor diffusion against a reservoir solution of PEG 4000 (10%) in MES (0.1 M, pH 6.0). The inhibitor complex of Compound 8 was achieved by soaking at an inhibitor concentration of 12 mM (6% DMSO) in 4000 PEG (9%) and MES (0.1 M, pH 5.5) using a drop ratio of 0.75:0.75. Compound 1 was soaked at an inhibitor concentration of 25 mM (12.5% DMSO) and 4000 PEG (12%) and MES (0.1 M, pH 5.25) using a drop ratio of 0.75:0.75. Crystals were cryoprotected with 25% glycerol in soaking solution and flash-frozen with liquid nitrogen. X-ray diffraction data were collected at 100 K at the Swiss Light Source (Villingen, Switzerland). Data were processed using XDS and XSCALE (18). Coordinates of BACE [PDB entry 2B8L (19)] were used for determination of phase information by molecular replacement. Subsequent model building and refinement were performed with CCP4 (20) and Coot (21). Ligand parametrization was conducted with ChemsSketch (version 10, ACD/Laboratories), and Libcheck (CCP4) was used for generation of the corresponding library files. We built the water model with the Find waters algorithm of Coot by putting water molecules in peaks of the  $F_o - F_c$  map contoured at  $3\sigma$  followed by refinement with Refmac 5.2 (22) and checking all waters with Coot. TLS (23) refinement was included toward the end using 12 TLS groups. All figures illustrating protein structures were generated using PyMOL (24).

## RESULTS

**BACE1 High-Throughput Fragment Screen (HTFS).** A homogeneous, fluorescence polarization assay was established to identify inhibitors of human BACE1 in a high-throughput fragment screen (HTFS). The read-out of this assay protocol is the difference in fluorescence polarization upon turnover of the substrate (Scheme 1). To validate this assay for high-concentration screening, we first evaluated known BACE1 inhibitors as a reference; both a high-affinity inhibitor and a low-affinity fragment were employed. Compound 7 had an IC<sub>50</sub> of  $45 \pm 17$  nM [BACE1 inhibitor IV (25)]. Compound 8 (3) had an inhibition of

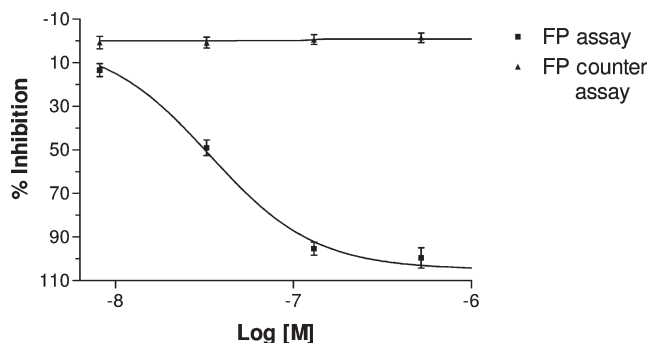


FIGURE 1: Concentration response curve of the high-affinity inhibitor. A concentration response in triplicate was measured for Compound 7 (Calbiochem BACE1 inhibitor IV) applying the fluorescence polarization (FP) assay. In the counterassay, where the compound is added after the cleavage reaction, no change in the assay read-out is observed.

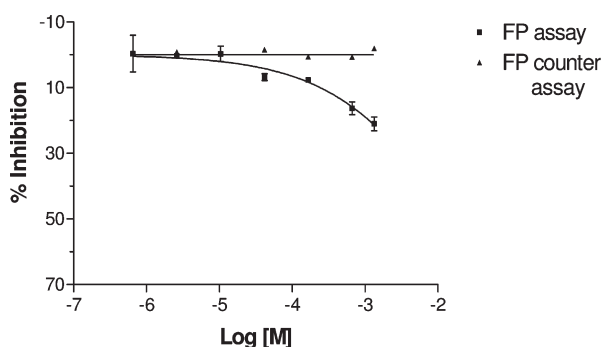


FIGURE 2: Concentration response curve of the low-affinity inhibitor. A concentration response in duplicate was measured for Compound 8 by applying the FP assay. In the counterassay, where the compound is added after the cleavage reaction, no change in the assay read-out is observed.

$24 \pm 7\%$  at a concentration of 1 mM. To confirm that the observed change in FP signal is indeed due to BACE1 inhibition (rather than interference of the compound with the assay read-out), a counterassay was established. Basically, the counterassay is performed in a manner similar to that of the primary screening assay, with the exception that the compound is added after the reaction has been stopped, instead of before the start of the reaction. If a compound leads to a decrease of the FP in the counterassay, it will be deemed a false positive hit. When applied to the counterassay, both BACE1 inhibitors, Compounds 7 and 8, did not interfere with the read-out (Figures 1 and 2). After validation of the assay for high-concentration screening, it was miniaturized to the 1  $\mu$ L format and adapted to the HTFS platform.

The HTFS with the ectodomain of BACE1 against a fragment library comprising 20000 compounds was performed with the DMSO-free NanoStore concept (26). The rationale behind the composition of the diverse fragment library has been described elsewhere (13, 27). Primary screening was performed at a compound concentration of 1 mM. Compound 7 was used as a positive control for normalization to 100%. The statistical quality was calculated from positive and negative control well replicates on the screening plates ( $Z' \sim 0.75$ ). The statistical hit threshold, calculated from the normalized assay signal values of the DMSO wells (sample negative controls), was set to  $3\sigma$  corresponding to 17% inhibition, thus allowing for sensitive detection of low-potency BACE1 inhibitors. On the basis of this,

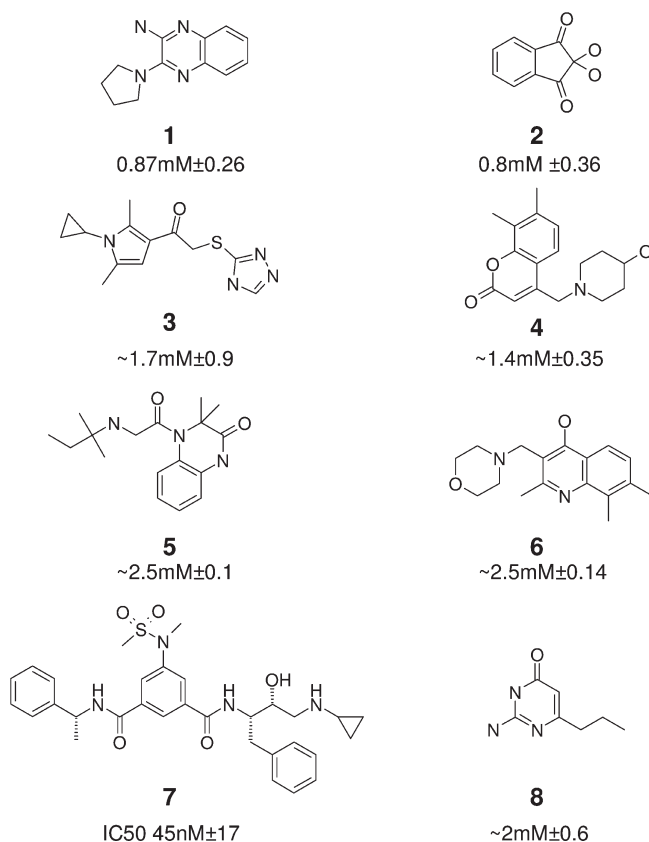


FIGURE 3: Some of the fragment hits confirmed by the assay cascade and Compound 7 (BACE1 inhibitor IV) distributed by Calbiochem (25) and Compound 8 published by Astra Zeneca (3).  $\text{IC}_{50}$  values are given with the standard deviation.

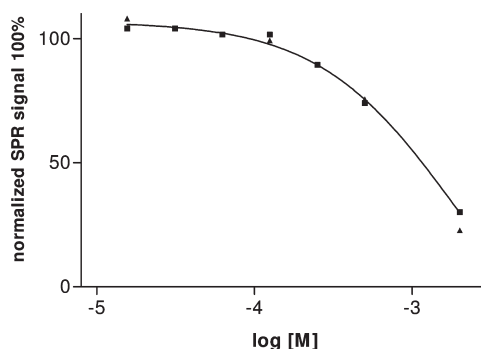


FIGURE 4: Inhibition in solution of interaction of BACE1/KEEI-SEVN-statin-VAEF with Compound 1 on a Biacore device. Data were fitted by nonlinear regression, and  $\text{IC}_{50}$  is estimated to be  $0.9 \pm 0.1$  mM ( $n = 2$ ). The maximum applied compound concentration is 2 mM; therefore, only a partial sigmoidal concentration response curve was recorded.

744 hits were selected for hit profiling and therefore tested against the primary BACE1 assay and the read-out artifact counterassay (0.01–1.8 mM). As a result, 60 profiled fragment hits were inactive in the counterassay and were taken forward for further analysis as potential BACE1 inhibitors.

**Hit Confirmation with the Secondary BACE1 Assay.** To further validate the remaining hit collection, an alternative BACE1 assay that is based on the functional reconstitution of  $\beta$ -galactosidase from an inactive subunit and a linear  $\alpha$ -complementation peptide was applied (commercially available as HitHunter  $\beta$ -secretase assay from GE-Healthcare). Briefly, the circular form of this peptide contains a BACE1 cleavage site but

Table 1: Data Collection and Refinement Statistics for the Crystal Structure of BACE1 with Compounds 1 and 8

	Compound 1	Compound 8
Data Collection		
space group	C2	C2
unit cell	$a = 230.63 \text{ \AA}$ , $b = 99.88 \text{ \AA}$ , $c = 62.90 \text{ \AA}$ , $\alpha = \gamma = 90^\circ$ , $\beta = 103.12^\circ$	$a = 232.55 \text{ \AA}$ , $b = 100.13 \text{ \AA}$ , $c = 64.78 \text{ \AA}$ , $\alpha =$ $\gamma = 90.00^\circ$ , $\beta = 103.73^\circ$
resolution ( $\text{\AA}$ ) (highest shell)	2.48 (2.54–2.48)	2.25 (2.44–2.25)
no. of unique reflections	48570 (4849)	66620 (13253)
completeness (%)	98.3 (98.0)	97.2 (89.9)
data cutoff [ $\sigma(F)$ ]	2.0	2.0
redundancy	3.3 (3.2)	3 (2.3)
$R_{\text{sym}}$ (%)	4.7 (43.9)	4.5 (34.7)
$R_{\text{meas}}$ (%)	5.6 (52.3)	5.4 (43.8)
mean $(I)/\sigma$	14.82 (3.01)	13.26 (2.65)
Model and Refinement		
$R_{\text{cryst}}$ (%)	22.6	22.2
$R_{\text{free}}$ (%)	28.1	26.5
rmsd for bond lengths ( $\text{\AA}$ )	0.010	0.011
rmsd for bond angles (deg)	1.21	1.15
rmsd for bonded B's ( $\text{\AA}^2$ )	1.3	0.9
no. of atoms per asymmetric unit	9066	8988
average $B$ factor ( $\text{\AA}^2$ )	20.7	29.7
protein (no. of atoms)	21.6 (8798)	31.3 (8844)
water (no. of atoms)	26.3 (117)	27.5 (180)
glycerol (no. of atoms)	58.9 (1)	40.2 (1)
ligand (no. of atoms)	43.5 (64)	52.5 (33)

is unable to complement. Upon cleavage of the circular peptide, the active  $\beta$ -galactosidase complex is formed able to hydrolyze its chromogenic substrate (15). Following a similar approach as described above, a read-out counterassay was applied allowing for the detection of false positive hits. Using a maximal compound concentration of 2 mM in a concentration response analysis, 26 fragment hits were confirmed with the alternative BACE1 assay protocol. IC<sub>50</sub> values of > 1 mM are estimated by extrapolation of an assumed sigmoidal concentration response. Representative hits are shown in Figure 3.

**Hit Confirmation with Surface Plasmon Resonance (SPR).** Before moving into X-ray crystallography studies, we assessed the binding mode of the hits via competition with known BACE1 inhibitors. Toward that end, we applied a SPR assay in which the BACE1 interaction partner had been immobilized on the sensor chip surface (3). The substrate analogue P<sub>10</sub>–P<sub>4</sub>/StatVal has been described to be an inhibitor of BACE1 (28) and serves as a probe for a defined binding site. In the cocrystal structure, P<sub>10</sub>–P<sub>4</sub>/StatVal interacts with residues P<sub>7</sub>–P<sub>4</sub>' covering the entire active site cleft of BACE1 (29). Thus, P<sub>10</sub>–P<sub>4</sub>/StatVal was applied as a reference for orthosteric inhibition of BACE1. BACE1 was kept at a constant concentration and preincubated with fragment hits. The ability of the protein to bind the immobilized ligand is determined by passing the mixture of BACE1 and fragment over the immobilized bait ligand surface. The magnitude of the binding signal decreases if a fragment hit is in competition with the specific binding site as shown for Compound 1 in Figure 4. The data were fitted by nonlinear regression, and the IC<sub>50</sub> was estimated to be  $0.9 \pm 0.1 \text{ mM}$  ( $n=2$ ).

**Structure of Compound 8 Bound to BACE1.** For further characterization of the binding mode of the fragments, high-quality apo BACE1 crystals were obtained and subjected to soaking experiments. We used Compound 8 for validation of the approach and soaked it into the BACE1 crystal. The crystal

diffracted to 2.25  $\text{\AA}$ , and the structure was determined by molecular replacement with a determined BACE1 structure. The crystal of space group C2 contained three monomers of BACE1 in the asymmetric unit with the same overall conformation (Table 1). The ligand bound in the active site is well-defined in the electron density in two of the three monomers per unit cell, and it adopts two different binding modes. The coordinate error as calculated with a Luzzati plot was 0.49  $\text{\AA}$ , and the occupancy in both monomers was 1.0. The exocyclic primary amine and the N1 atom in the core of Compound 8 form four specific hydrogen bonds with BACE1, namely, to the side chain carboxyl of Asp32 and Asp228. In monomer 1, an additional hydrogen bond between the ligand carbonyl and the main chain nitrogen of Gln73 in the flap is formed, which contributes to the flap closed conformation in this monomer (Figure 5). In the second binding mode of Compound 8, the heterocycle is flipped by approximately 180°, retaining the interaction with the catalytic aspartate residues but losing the backbone interaction with Gln73 in the flap of BACE1. Accordingly, the flap is in an open conformation with Thr72 in this monomer displaced by 3.2  $\text{\AA}$  from its position in the first monomer. Electron density for Thr72 is clearly defined, as shown for monomer 1 in Figure 5d. The third monomer without a ligand in the binding site is also in a flap open conformation.

**Structure of Compound 1 Bound to BACE1.** A BACE1 crystal soaked with Compound 1 diffracted to 2.48  $\text{\AA}$  (Table 1). The ligand is bound in the active site with an occupancy in monomers 1 and 3 of 0.7, and the coordinate error determined with a Luzzati plot was 0.56  $\text{\AA}$ . In both monomers, the ligand had the same orientation, and the electron density of the ligand is well-reflected in the central heterocycle and the pyrrolidine moiety but has some gaps in the benzyl ring pointing toward the flap (Figure 6a). There are four hydrogen bonds (shown as dashed lines in Figure 6b) between the exocyclic primary amine



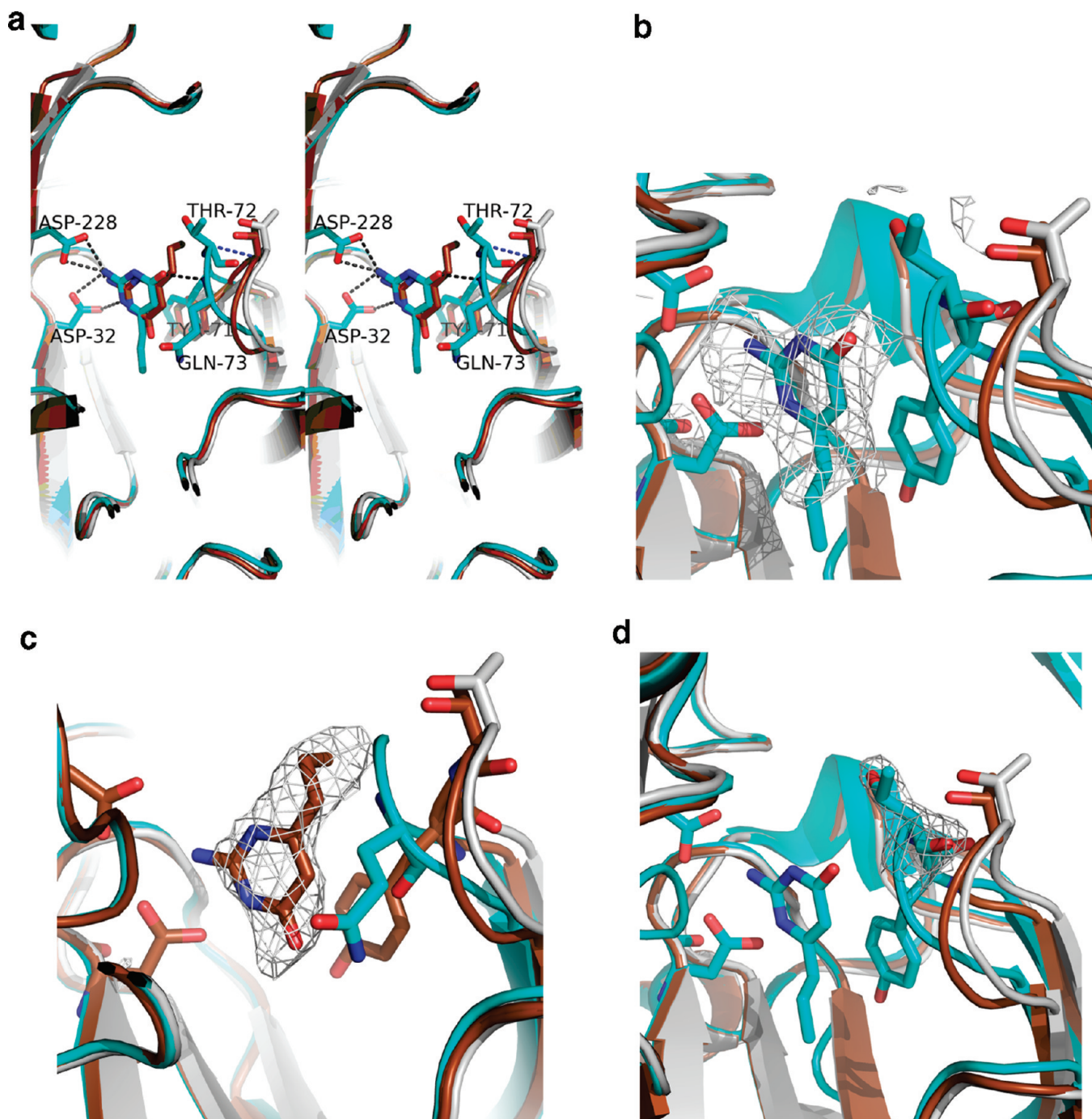


FIGURE 5: Compound 8 bound to BACE1. (a) Alignment of monomers 1 (blue), 2 (brown), and 3 (gray) as stereo pictures. There are four hydrogen bonds (shown as dashed lines) between Compound 8 and the active site aspartic acids. The fifth hydrogen bond is present between the ligand and the backbone nitrogen of Gln73 in the flap in monomer 1. C $\alpha$  of Thr72 in the flap is 3.2 Å apart in monomers 1 and 2, indicated by the blue dashed line. Monomer 3 does not contain the ligand, and its flap is in a position similar to that of monomer 2. Carbon atoms are colored light blue/brown, oxygen atoms red, and nitrogen atoms dark blue. (b and c) The  $F_o - F_c$  difference density of the ligand contoured at  $2\sigma$  in monomers 1 and 2. (d) The  $2F_o - F_c$  difference density of Thr72 contoured at  $1\sigma$  in monomer 1.

and the N1 atom in the core of Compound 1 and the carboxyls of the active site aspartic acids. A further face-to-edge  $\pi$ -stacking interaction is identified between the benzyl of Compound 1 and the phenyl ring of Tyr71. The pyrrolidine of Compound 1 is pointing toward the S1' pocket of BACE1. There is the possibility of a weak electrostatic interaction between the tertiary amine of Compound 1 and either the carboxyl of Asp228 or the hydroxyl of Thr231, both being 3.5 and 4 Å apart. We also found the ligand present in monomer 2 with a low occupancy, but the fit to the electron density was not conclusive. Electron density for the flap

residues in monomer 2 was not well-defined, and therefore, this region was excluded from the model.

**Structure–Activity Relationship (SAR) of Compound 1.** A range of commercial compounds were selected that would confirm the observed binding mode of Compound 1 and possibly explore synthetic vectors for improving potency. The selected compounds were purchased from external suppliers, and their identity and purity were confirmed by liquid chromatography–mass spectroscopy (LC–MS) analysis. Potency of the compounds was evaluated by the HitHunter assay using two or three

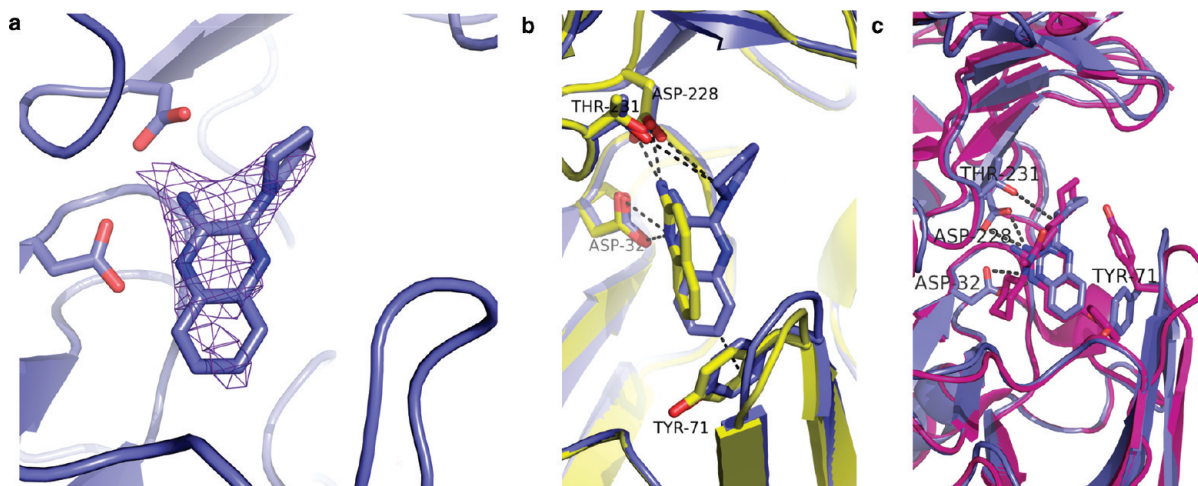


FIGURE 6: Compound 1 bound to BACE1. (A) Alignment of monomers 1 (blue), 2 (orange), and 3 (green). Hydrogen bonds between Compound 1 and the active site aspartic acids are shown as dashed lines. A further face-to-edge  $\pi$ -stacking interaction is formed between the benzyl ring of Compound 1 and the phenyl ring of Tyr71. The pyrrolidine of Compound 1 is pointing toward the S1' pocket of BACE1. (B) The  $F_o - F_c$  difference density of the ligand contoured at  $2\sigma$  in monomer 3. (C) Alignment of Compound 1 monomer 3 (blue) with aminoquinoline (yellow) [PDB entry 2OHL (5)]. (D) Alignment of Compound 1 monomer 3 (blue) with dihydroquinazoline (magenta) [PDB entry 2Q15 (30)].

independent concentration response curves (0.03–2 mM) each in triplicate (Table 2). Within this concentration range,  $IC_{50}$  values of up to 1 mM could be accurately determined.  $IC_{50}$  values of  $> 1$  mM are estimated by extrapolation of an assumed sigmoidal concentration response with 100% inhibition (standard deviation in parentheses). Ligand efficiency (LE) is a useful concept for measuring the effectiveness of compound optimization, and we report it here as  $-RT \ln(IC_{50})/(\text{none H atom count})$  (2). Compound 16 improved in potency and LE compared to Compound 1.

## DISCUSSION

By applying a highly diverse fragment library for screening, we aimed to discover novel BACE1 inhibitors. We demonstrate here that low-affinity BACE1 fragment inhibitors can readily be identified by biochemical screening methods and that these inhibitors are suitable for studying the detailed binding mode by X-ray crystallography. The identified hit collection exhibited broad chemical diversity as demonstrated in Figure 3.

Further characterization of Compound 1 and experimental fragment hits in the SPR assay led to the conclusion that their mode of inhibition was competitive. Compounds 1 and 8 had been selected for crystallization trials because of their favorable molecular weight to potency ratio. Soaking as well as cocrystallization was tried, but only soaking was successful. The chemical properties of both compounds probably limited success in cocrystallization trials.

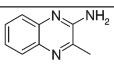
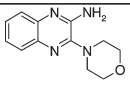
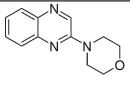
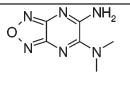
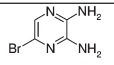
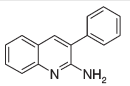
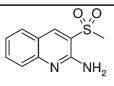
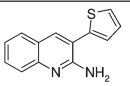
Aminoquinolines in complex with BACE1 have been published recently (5), and alignment of our Compound 1 crystal structure with an aminoquinoline fragment (PDB entry 2OHL) is depicted in Figure 6b. The modes of binding of the cores of both compounds to the catalytic aspartates and to Tyr71 are very similar; however, the plane of the core of Compound 1 is twisted by approximately  $30^\circ$  toward the prime side of the active site cleft when compared to the core in 2OHL. An additional interaction mediated either by the pyrrolidine moiety or by the second tertiary amine in the central heterocycle may be the reason for this alternative position in Compound 1. An alignment of Compound 1 with another aminoquinazoline [PDB entry 2Q15 (30)] reveals the same planar position of the heterocyclic core (Figure 6c). Here, the pyrrolidine of Compound 1 overlaps

well with the cyclohexyl of the 2Q15 ligand, suggesting a preference for hydrophobic substituents in this part of the BACE1 S1' region. The ligand occupancy of 0.7 in monomers 1 and 3 may account for the partial electron density in the benzyl pointing toward the flap. In monomer 2, the ligand is possibly present as two different conformers, but each at a low occupancy of  $< 0.5$ . In addition, the flap region is disordered in this monomer, making interpretation of the results difficult. Therefore, we focused on the ligand orientation present in monomers 1 and 3, as these are corroborated by published protein ligand structures.

Both ligands, Compounds 1 and 8, interact in a similar manner with the catalytic aspartate residues, while the interaction with the flap distinguishes the binding mode of the compounds. Compound 1 interacts with Tyr71, thus contributing to keeping the flap in an open conformation, whereas the backbone interaction of Compound 8 with Gln73 contributes to the closure of the flap which leads to a 3.2 Å shift in the position of the C $\alpha$  atom of the flap residue Thr72 (Figure 7). Temperature values of Thr72 are not increased in the flap open compared to the closed conformation, but they are increased in monomer 2 compared to monomers 1 and 3. The average  $B$  factors of Thr72 in the flap region of the Compound 1 ligand complex are 23.5 for monomers 1 and 3, indicating that they are well-ordered while Thr72 of monomer 2 is disordered in this region. A similar pattern is observed in the Compound 8 crystal structure where Thr72 residues in monomers 1 and 3 have lower  $B$  factors (24.4 and 27.3, respectively) than in monomer 2 (33.7). This may be a feature of the crystal system as the flaps of monomers 1 and 3 are well-defined in the electron density when compared to monomer 2. The higher flexibility may also account for the second binding mode for Compound 8 observed in monomer 2. For this monomer, we also found Compound 8 with 100% occupancy bound to the protein surface close to the C-terminus interacting with residues Lys218, Gln219, Tyr222, and Tyr384. We assume that this is an artifact caused by the applied crystal system rather than an allosteric site, because it did not induce obvious conformational changes to the protein and we observed it in only one of the monomers.

The flap closed conformation of Compound 8 aligns well with published flap closed BACE1 conformations, e.g., PDB entry

Table 2: Structure–Activity Relationship (SAR) of Analogues of Compound 1

Compound	Structure	IC <sub>50</sub> BACE1	LE
9		~2.7mM (±0.8)	0.30
10		0.97mM (±0.03)	0.25
11		>5mM	-
12		>5mM	-
13		~2.1mM (±0.09)	0.42
14		~2.8mM (±0.82)	0.21
15		~3.6mM (±1.3)	0.23
16		0.41mM (±0.03)	0.30

1W51 (11). The flap open conformation present in complexes of Compounds 1 and 8 (monomers 2 and 3) does not match entirely with the flap in the apo structure 1W50 (11), indicating that the flap of BACE1 in our crystal system is not fully open. A full transition between the open and closed conformation is reported with a distance of 4.5 Å at the tip of the flap (10, 11).

Multiple binding modes were observed in the protein ligand structure of Compound 8. This might be inherent to small fragments with a degree of internal symmetry, in particular where the main contributor for binding is a single functional group. Adoption of more than one conformation of the ligand in the active site is reported, for example, for  $\beta$ -lactamase (31) and HIV1 reverse transcriptase (32). We can expect that through structure-guided optimization of Compound 8, where additional functional groups will be introduced, specific residues in the active site will pick up additional contacts within the active site of BACE1, thus restricting the degree of freedom of the inhibitor to a single binding mode (31). Analogues of Compound 8 with a higher affinity for BACE1 [PDB entry 2VA5 (7)] are favoring the binding mode observed in monomer 1. The second binding mode

observed in monomer 2 has not been reported in the literature yet and might open new opportunities for optimization of this class of BACE1 inhibitors.

For Compound 1, we have demonstrated how a preliminary SAR can be established using commercially available analogues. Replacement of the pyrrolidine motif of compound 1 with methyl as with Compound 9 results in a drop in potency probably due to the loss of the weak H-bond interaction between the pyrrolidine and Asp228/Thr231. Replacement of the pyrrolidine motif of compound 1 with the structurally similar morpholine results in the essentially equipotent Compound 10 and suggests that additional analogues of this compound could be synthesized that might pick up interactions with residues such as Arg235 at the top of the S2 pocket, a strategy successfully employed by Petukhov (33). Deletion of the primary amine as in Compound 11 leads to a complete loss of BACE1 activity, confirming the observed interaction with the catalytic aspartates in the crystal structure. Replacement of the phenyl ring of the quinoxaline and truncation of the pyrrolidine to a dimethylamine, as shown in Compound 12, or truncation to the primary amine as in



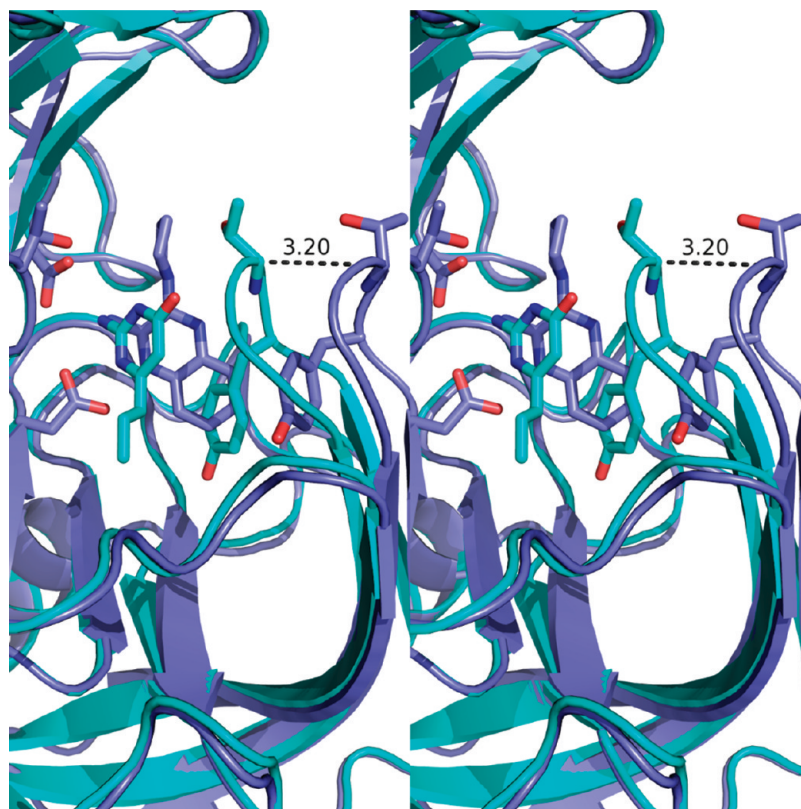


FIGURE 7: Compounds 1 and 8 overlaid in the catalytic site of BACE1. (A) Alignment of Compound 1 monomer 1 (dark blue) and Compound 8 monomer 1 (light blue). Both ligands are interacting in a similar manner with the catalytic aspartates. Interaction with the flap is different leading to an open (Compound 1) and closed (Compound 8) flap conformation with Thr72 3.2 Å apart at the top of the loop.

Compound 13, result in a loss or reduction of BACE1 activity, suggesting that the  $\pi$ -interaction of the phenyl ring with Tyr71 located in the flap is sensitive to such changes. In the crystal structure, the second endocyclic nitrogen of Compound 1, pointing toward the flap, is not interacting with BACE1 residues in an obvious manner (Figure 6). Therefore, three compounds in which this endocyclic nitrogen was deleted were purchased, leading to some 2-aminoquinolines reminiscent of fragment hits reported by Astex on their BACE1 program (6). In our hands, one of these heterocycles, Compound 16, underwent an increase in potency compared to compound 1; however, the closely related compound 14 lost potency. Concomitant with the potency increase of Compound 16, LE improved from 0.27 to 0.3, qualifying this compound as a promising starting point for the development of an orally available drug candidate (2). Although the affinities of fragment inhibitors are not sufficiently high to warrant the collection of in vitro ADME (absorption, distribution, metabolism, and excretion) data for potential in vivo experiments, we investigated their in silico properties to gain an understanding of their likely behavior in vivo. The topological polar surface area (TPSA) of a compound is a good predictor for blood–brain barrier (BBB) penetration, and values of  $< 60\text{--}70\text{ \AA}^2$  should allow entry of the compound into the brain (34). Oral bioavailability could be predicted by the Veber algorithm (35). Compounds 1 and 16 are predicted to cross the BBB and be orally bioavailable because they have TPSA values of 55 and 39 and pass the Veber bioavailability filter. Although these are encouraging predictions, we have to keep in mind that optimization of fragment hits using structure-guided techniques such as crystallography does increase the molecular weight and TPSA, factors that can have an impact on the likelihood of BBB penetration.

In conclusion, we have demonstrated the identification of BACE1 fragment inhibitors by biochemical screening methods, being potential starting points for the development of orally bioavailable and brain penetrant drug candidates. We highlight the importance of obtaining protein ligand and crystal structures as a strategy for identifying the binding mode and growth vectors for the optimization of low-affinity micromolar fragments into high-affinity nanomolar leads. In the absence of crystallographic data, it may be possible to explore the SAR of fragment hits using commercially available analogues in combination with techniques such as SPR.

## ACKNOWLEDGMENT

We thank Christian Kirchhoff, Pierre Ilouga, Dirk Winkler, Marcus Janssen, Stefanie Haase, and Marion Biniszkiwicz for helpful assistance and support. We also acknowledge Yong-Hwa Song from EMBL Hamburg (Hamburg, Germany) and Prof. Rainer Rudolph from Halle-Wittenberg University (Halle, Germany) for help with protein refolding.

## REFERENCES

- Hesterkamp, T., and Whittaker, M. (2008) Fragment-based activity space: Smaller is better. *Curr. Opin. Chem. Biol.* 12, 260–268.
- Congreve, M., Chessari, G., Tisi, D., and Woodhead, A. J. (2008) Recent developments in fragment-based drug discovery. *J. Med. Chem.* 51, 3661–3680.
- Geschwindner, S., Olsson, L. L., Albert, J. S., Deinum, J., Edwards, P. D., de Beer, T., and Folmer, R. H. (2007) Discovery of a novel warhead against  $\beta$ -secretase through fragment-based lead generation. *J. Med. Chem.* 50, 5903–5911.
- Kuglstatter, A., Stahl, M., Peters, J. U., Huber, W., Stihle, M., Schlatter, D., Benz, J., Ruf, A., Roth, D., Enderle, T., and Hennig,



- M. (2008) Tyramine fragment binding to BACE-1. *Bioorg. Med. Chem. Lett.* 18, 1304–1307.
5. Murray, C. W., Callaghan, O., Chessari, G., Cleasby, A., Congreve, M., Frederickson, M., Hartshorn, M. J., McMenamin, R., Patel, S., and Wallis, N. (2007) Application of fragment screening by X-ray crystallography to  $\beta$ -secretase. *J. Med. Chem.* 50, 1116–1123.
6. Congreve, M., Aharony, D., Albert, J., Callaghan, O., Campbell, J., Carr, R. A., Chessari, G., Cowan, S., Edwards, P. D., Frederickson, M., McMenamin, R., Murray, C. W., Patel, S., and Wallis, N. (2007) Application of fragment screening by X-ray crystallography to the discovery of aminopyridines as inhibitors of  $\beta$ -secretase. *J. Med. Chem.* 50, 1124–1132.
7. Edwards, P. D., Albert, J. S., Sylvester, M., Aharony, D., Andisik, D., Callaghan, O., Campbell, J. B., Carr, R. A., Chessari, G., Congreve, M., Frederickson, M., Folmer, R. H., Geschwindner, S., Koether, G., Kolmodin, K., Krumrine, J., Mauger, R. C., Murray, C. W., Olsson, L. L., Patel, S., Spear, N., and Tian, G. (2007) Application of fragment-based lead generation to the discovery of novel, cyclic amidine  $\beta$ -secretase inhibitors with nanomolar potency, cellular activity, and high ligand efficiency. *J. Med. Chem.* 50, 5912–5925.
8. Yang, W., Fucini, R. V., Fahr, B. T., Randal, M., Lind, K. E., Lam, M. B., Lu, W., Lu, Y., Cary, D. R., Romanowski, M. J., Colussi, D., Pietrak, B., Allison, T. J., Munshi, S. K., Penny, D. M., Pham, P., Sun, J., Thomas, A. E., Wilkinson, J. M., Jacobs, J. W., McDowell, R. S., and Ballinger, M. D. (2009) Fragment-Based Discovery of Nonpeptidic BACE-1 Inhibitors Using Tethering. *Biochemistry* 48, 4488–4496.
9. Hong, L., Koelsch, G., Lin, X., Wu, S., Terzyan, S., Ghosh, A. K., Zhang, X. C., and Tang, J. (2000) Structure of the protease domain of memapsin 2 ( $\beta$ -secretase) complexed with inhibitor. *Science* 290, 150–153.
10. Hong, L., and Tang, J. (2004) Flap position of free memapsin 2 ( $\beta$ -secretase), a model for flap opening in aspartic protease catalysis. *Biochemistry* 43, 4689–4695.
11. Patel, S., Vuillard, L., Cleasby, A., Murray, C. W., and Yon, J. (2004) Apo and inhibitor complex structures of BACE ( $\beta$ -secretase). *J. Mol. Biol.* 343, 407–416.
12. Steele, T. G., Hills, I. D., Nomland, A. A., de León, P., Allison, T., McGaughey, G., Colussi, D., Tugusheva, K., Haugabook, S. J., Espeseth, A. S., Zuck, P., Graham, S. L., and Stachel, S. J. (2009) Identification of a small molecule  $\beta$ -secretase inhibitor that binds without catalytic aspartate engagement. *Bioorg. Med. Chem. Lett.* 19, 17–20.
13. Hestekamp, T., Barker, J., Davenport, A., and Whittaker, M. (2007) Fragment based drug discovery using fluorescence correlation: Spectroscopy techniques: Challenges and solutions. *Curr. Top. Med. Chem.* 7, 1582–1591.
14. Haass, C., Lemere, C. A., Capell, A., Citron, M., Seubert, P., Schenk, D., Lannfelt, L., and Selkoe, D. J. (1995) The Swedish mutation causes early-onset Alzheimer's disease by  $\beta$ -secretase cleavage within the secretory pathway. *Nat. Med.* 1, 1291–1296.
15. Naqvi, T., Lim, A., Rouhani, R., Singh, R., and Eglen, R. M. (2004)  $\beta$ -Galactosidase enzyme fragment complementation as a high-throughput screening protease technology. *J. Biomol. Screening* 9, 398–408.
16. Hanessian, S., Yun, H., Hou, Y., Yang, G., Bayrakdarian, M., Therrien, E., Moitessier, N., Roggo, S., Veenstra, S., Tinteln-Blomley, M., Rondeau, J. M., Ostermeier, C., Strauss, A., Ramage, P., Paganetti, P., Neumann, U., and Betschart, C. (2005) Structure-based design, synthesis, and memapsin 2 (BACE) inhibitory activity of carbocyclic and heterocyclic peptidomimetics. *J. Med. Chem.* 48, 5175–5190.
17. Barazza, A., Gotz, M., Cadamuro, S. A., Goettig, P., Willem, M., Steuber, H., Kohler, T., Jestel, A., Reinemer, P., Renner, C., Bode, W., and Moroder, L. (2007) Macrocyclic statine-based inhibitors of BACE-1. *ChemBioChem* 8, 2078–2091.
18. Kabsch, W. (1993) Automatic processing of rotation diffraction data from crystals of initially unknown symmetry and cell constants. *J. Appl. Crystallogr.* 26, 795–800.
19. Stachel, S. J., Coburn, C. A., Steele, T. G., Crouthamel, M. C., Pietrak, B. L., Lai, M. T., Holloway, M. K., Munshi, S. K., Graham, S. L., and Vacca, J. P. (2006) Conformationally biased P3 amide replacements of  $\beta$ -secretase inhibitors. *Bioorg. Med. Chem. Lett.* 16, 641–644.
20. Collaborative Computational Project No. 4 (1994) The CCP4 suite: Programs for protein crystallography. *Acta Crystallogr. D* 50, 760–763.
21. Emsley, P., and Cowtan, K. (2004) Coot: Model-building tools for molecular graphics. *Acta Crystallogr. D* 60, 2126–2132.
22. Murshudov, G. N., Vagin, A. A., and Dodson, E. J. (1997) Refinement of macromolecular structures by the maximum-likelihood method. *Acta Crystallogr. D* 53, 240–255.
23. Winn, M. D., Isupov, M. N., and Murshudov, G. N. (2001) Use of TLS parameters to model anisotropic displacements in macromolecular refinement. *Acta Crystallogr. D* 57, 122–133.
24. DeLano, W. L. (2006) The PyMOL Molecular Graphics System, DeLano Scientific LLC, San Carlos, CA.
25. Stachel, S. J., Coburn, C. A., Steele, T. G., Jones, K. G., Loutzenhiser, E. F., Grego, A. R., Rajapakse, H. A., Lai, M. T., Crouthamel, M. C., Xu, M., Tugusheva, K., Lineberger, J. E., Pietrak, B. L., Espeseth, A. S., Shi, X. P., Chen-Dodson, E., Holloway, M. K., Munshi, S., Simon, A. J., Kuo, L., and Vacca, J. P. (2004) Structure-based design of potent and selective cell-permeable inhibitors of human  $\beta$ -secretase (BACE-1). *J. Med. Chem.* 47, 6447–6450.
26. Benson, N., Boyd, H. F., Everett, J. R., Fries, J., Gribbon, P., Haque, N., Henco, K., Jessen, T., Martin, W. H., Mathewson, T. J., Sharp, R. E., Spencer, R. W., Stuhmeier, F., Wallace, M. S., and Winkler, D. (2005) NanoStore: A concept for logistical improvements of compound handling in high-throughput screening. *J. Biomol. Screening* 10, 573–580.
27. Barker, J., Courtney, S., Hestekamp, T., and Whittaker, M. (2006) Fragment screening by biochemical assay. *Expert Opin. Drug Discovery* 1, 225–236.
28. Sinha, S., Anderson, J. P., Barbour, R., Basi, G. S., Caccavello, R., Davis, D., Doan, M., Dovey, H. F., Frigon, N., Hong, J., Jacobson-Croak, K., Jewett, N., Keim, P., Knops, J., Lieberburg, I., Power, M., Tan, H., Tatsuno, G., Tung, J., Schenk, D., Seubert, P., Suomensaar, S. M., Wang, S., Walker, D., Zhao, J., McConlogue, L., and John, V. (1999) Purification and cloning of amyloid precursor protein  $\beta$ -secretase from human brain. *Nature* 402, 537–540.
29. Turner, R. T., III, Hong, L., Koelsch, G., Ghosh, A. K., and Tang, J. (2005) Structural locations and functional roles of new subsites S5, S6, and S7 in memapsin 2 ( $\beta$ -secretase). *Biochemistry* 44, 105–112.
30. Baxter, E. W., Conway, K. A., Kennis, L., Bischoff, F., Mercken, M. H., Winter, H. L., Reynolds, C. H., Tounge, B. A., Luo, C., Scott, M. K., Huang, Y., Braeken, M., Pieters, S. M., Berthelot, D. J., Masure, S., Bruinzeel, W. D., Jordan, A. D., Parker, M. H., Boyd, R. E., Qu, J., Alexander, R. S., Brenneeman, D. E., and Reitz, A. B. (2007) 2-Amino-3,4-dihydroquinazolines as inhibitors of BACE-1 ( $\beta$ -site APP cleaving enzyme): Use of structure based design to convert a micromolar hit into a nanomolar lead. *J. Med. Chem.* 50, 4261–4264.
31. Babaoglu, K., and Shoichet, B. K. (2006) Deconstructing fragment-based inhibitor discovery. *Nat. Chem. Biol.* 2, 720–723.
32. Lewi, P. J., de, J. M., Daeyaert, F., Koymans, L., Vinkers, M., Heeres, J., Janssen, P. A., Arnold, E., Das, K., Clark, A. D., Jr., Hughes, S. H., Boyer, P. L., de Bethune, M. P., Pauwels, R., Andries, K., Kukla, M., Ludovici, D., De Corte, B., Kavash, R., and Ho, C. (2003) On the detection of multiple-binding modes of ligands to proteins, from biological, structural, and modeling data. *J. Comput.-Aided Mol. Des.* 17, 129–134.
33. Chirapu, S. R., Pachaiyappan, B., Nural, H. F., Cheng, X., Yuan, H., Lankin, D. C., Abdul-Hay, S. O., Thatcher, G. R., Shen, Y., Kozikowski, A. P., and Petukhov, P. A. (2009) Molecular modeling, synthesis, and activity studies of novel biaryl and fused-ring BACE1 inhibitors. *Bioorg. Med. Chem. Lett.* 19, 264–274.
34. Ertl, P., Rohde, B., and Selzer, P. (2000) Fast calculation of molecular polar surface area as a sum of fragment-based contributions and its application to the prediction of drug transport properties. *J. Med. Chem.* 43, 3714–3717.
35. Veber, D. F., Johnson, S. R., Cheng, H. Y., Smith, B. R., Ward, K. W., and Kopple, K. D. (2002) Molecular properties that influence the oral bioavailability of drug candidates. *J. Med. Chem.* 45, 2615–2623.